Optimal control for electromagnetic haptic guidance systems

Optimal Control for Electromagnetic Haptic Guidance Systems

Thomas Langerak[1], **Juan José Zárate**[1], **Velko Vechev**[1], **David Lindlbauer**[1], **Daniele Panozzo**[2], **Otmar Hilliges**[1]
[1] Department of Computer Science, ETH Zurich, Zurich, Switzerland
[2] Courant Institute of Mathematical Sciences, New York University, New York, USA

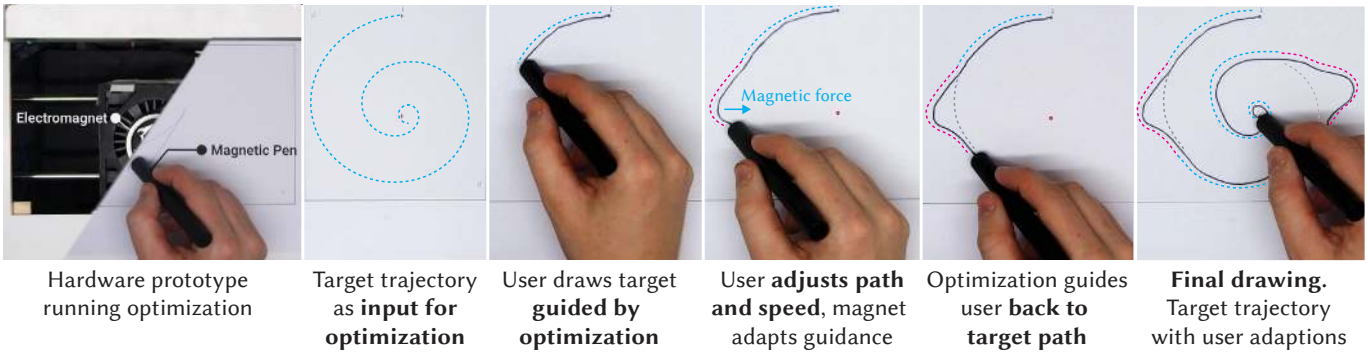

Figure 1. We propose an optimal control scheme for electromagnetic guidance systems (*left*). A target trajectory is provided, on which users are guided. They can always adapt the trajectory, our optimization then guides users back to the target (*offset between target and drawing for illustration purposes*).

ABSTRACT

We introduce an optimal control method for electromagnetic haptic guidance systems. Our real-time approach assists users in pen-based tasks such as drawing, sketching or designing. The key to our control method is that it guides users, yet does not take away agency. Existing approaches force the stylus to a continuously advancing setpoint on a target trajectory, leading to undesirable behavior such as loss of haptic guidance or unintended snapping. Our control approach, in contrast, gently pulls users towards the target trajectory, allowing them to always easily override the system to adapt their input spontaneously and draw at their own speed. To achieve this flexible guidance, our optimization iteratively predicts the motion of an input device such as a pen, and adjusts the position and strength of an underlying dynamic electromagnetic actuator accordingly. To enable real-time computation, we additionally introduce a novel and fast approximate model of an electromagnet. We demonstrate the applicability of our approach by implementing it on a prototypical hardware platform based on an electromagnet moving on a bi-axial linear stage, as well as a set of applications. Experimental results show that our approach is more accurate and preferred by users compared to open-loop and time-dependent closed-loop approaches.

Author Keywords

Optimal control; Computational Interaction; Haptic devices;

UIST '20, October 20–23, 2020, Virtual Event, USA

ACM ISBN 978-1-4503-7514-6/20/10 ...$15.00.
http://dx.doi.org/10.1145/3379337.3415593

CCS Concepts

•**Human-centered computing** → **Haptic devices;** •**Hardware** → **Haptic devices;**

INTRODUCTION

Pen-based interactive systems that feature *haptic guidance* support users in a variety of applications such as drawing, sketching, writing or CAD design. The goal of such systems is to enable users to draw higher-complexity shapes with less effort and higher accuracy, or to support users through virtual haptic tools such as rulers or guides. Crucially, such systems aim to strike a balance between giving users a strong sense of control and agency, while providing feedback unobtrusively. This is enabled through embedding controllable electromagnets in the system, for example, which can then guide input devices such as a pen, or provide feedback to users about the positions and boundaries of virtual objects.

Existing systems such as dePenD [39] typically employ an *open-loop control approach*. The magnet that drives the pen is set to a predefined trajectory, and users then must closely follow the movement of the system. In this case, it is not possible for users to adjust the trajectory, since it would lead to a loss of haptic guidance. This effectively leads to a decrease in control of users, and arguably a loss of user agency. Alternatively, it is possible to extend haptic guidance systems with traditional closed-loop approaches, e. g. by implementing a proportional–integral–derivative (PID) controller [4] or based on heuristics [21]. Such systems adjust to users' movement but are, usually, based on a timed reference, effectively dictating users' drawing speed. This can lead to unintended behavior such as snapping whenever the pen is too close to the actuator, a problem that is exacerbated for magnetic systems due to the non-linear nature of the magnetic force over distance.

We propose a real-time closed-loop control approach that allows users to retain agency and control while being assisted by an electromagnetic haptic guidance system. Our approach enables users to draw at their desired speed and adjust their target trajectory continuously. It then adapts and complies to such modifications while giving corrective feedback. Our algorithm then positions and regulates a variable-strength electromagnet such that it provides dynamically adjustable in-plane magnetic forces to the pen tip.

We contribute a novel optimization scheme for electromagnetic-based haptic guidance system, i. e. models and control algorithm, that enables formalizing this problem in the established Model Predictive Contour Control (MPCC) framework [16], which has previously only been employed in context such as RC-racing [20] or drone cinematography [26]. We provide an accurate system model, parameters, and an appropriate cost function alongside a method to optimize the model parameters given user inputs. Modeling the non-linear interaction of an electromagnetic force field typically makes use of the finite element method (FEM), which is not applicable for real-time scenarios. To overcome this challenge, we additionally contribute a novel approximate yet accurate model of the electromagnetic force field that can be evaluated analytically in real time.

Compared to simpler control schemes such as Model Predictive Control (MPC) [8] and many implementations of PID control, our approach does not require a timed reference and hence allows users to draw at their desired speed. Furthermore, our optimization scheme allows for error-correcting force feedback, gently pulling the user back to the desired trajectory rather than pushing or pulling the pen to a continuously advancing setpoint on the trajectory. With our approach, the reference path can be updated at every timestep, thus allowing users to continuously change their desired trajectories. This enables applying the algorithm to fully dynamic references, for example virtual tools such as rulers or programmable french curves.

To assess the proposed control algorithm, we developed a proof-of-concept hardware implementation (see Figure 2), leveraging an electromagnet that moves underneath the drawing surface or display on a bi-axial linear stage. The magnet provides variable strength guidance onto the tip of a minimally instrumented pen or stylus via an electromagnet positioned directly below a drawing surface, guided by our proposed approach. We demonstrate the feasibility of our approach with a set of applications, specifically drawing guidance on conventional paper for sketching and writing, and a digital sketching application that features virtual haptic guides and rulers.

To evaluate our approach, we performed two experiments with twelve participants each. We first compared free-hand drawing of shapes with varying complexity with and without our feedback system. Results showed that the haptic guidance using our approach improved the accuracy across shapes by up to 50% to 1.87 mm. We then compared our approach to our implementation of dePENd (open-loop) and a simple MPC-based closed-loop control scheme. Our approach showed significantly higher accuracy, and was preferred by users.

In summary, we contribute

- A novel MPCC-based optimization scheme for electromagnetic haptic guidance systems including models, parameters, cost function and control algorithm.
- A novel real-time approximate model for electromagnets that generalizes beyond our hardware implementation.
- Evaluations showing the improved accuracy of our method.
- A prototypical software and hardware implementation available as open source at https://ait.ethz.ch/projects/2020/magpen/.

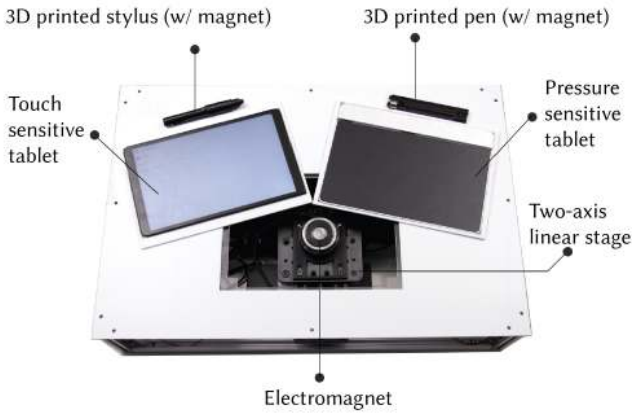

Figure 2. We implement our proposed guidance system using a two-axis linear stage equipped with an electromagnet. All technical and user evaluations were completed using the Pressure Sensitive Tablet (*right*). We additionally developed an all-digital implementation using a multi-touch tablet with display (*left*).

RELATED WORK

Haptic guidance

Providing haptic guidance to users can provide benefits for learning [36] and short-term performance (cf. Abbink et al. [1]). Teranishi et al. [36] demonstrate that participants showed improved learning for handwriting skills when receiving guidance through a 3-DOF Phantom Omni device. Mullin et al. [25] use a similar device as handwriting aid for rehabilitation. Forsynth and MacLean [10] show that force cues are beneficial in navigation tasks. The focus of these works is that users receive tight guidance (i. e. they are supposed to follow the system as closely as possible). Our work aims at providing a control strategy that allows users to deviate from predefined trajectories while still receiving guidance.

There exists a large range of devices and systems that aim at providing guidance to users. Comp*Pass [27] uses pantograph-like devices to assist users in drawing, while I-Draw [9] is a motorized drawing assistant. Lin et al. [19] use a magnet mounted on a small robotic arm to retain the correspondence between the pen and a portable base. Digital rubbing employs a comparable system using a solenoid for tracing over digital images on real paper [14]. While users handle larger-scale motions of the devices, they generally aim at having full control over the resulting drawing. Users can take back this control, however these system do not provide a way to guide users back to the target trajectory. Besides aforementioned systems,

several works aid users in the process of crafting and manufacturing (cf. Zoran et al. [44]). Free-D [43] and D-Coil [29] assist users in sculpting of physical artefacts by guiding them on a predefined 3D shape. Shilkrot et al. [31] proposes an augmented paint brush to assist users in painting. While users can override these systems to deviate from the target shape, they have no mechanism that guides users back to the target.

Closest to our work in terms of hardware is dePENd by Yamaoka et al. [39]. They move a permanent neodymium magnet on a two-axis setup to control the metal tip of a ballpoint pen. The neodymium magnet "drags" the input pen around a predefined path, similar to a plotter. dePENd employs an open-loop strategy to control the magnet, which means users cannot deviate from the predefined path without risking to lose haptic guidance. We propose a mathematical model and optimal control strategy that allows users to move at their own pace through a drawing, for example, and reacts in real-time to user input by altering the position and strength of the magnet. We show that our approach provides better results than their open-loop approach, as well as existing closed-loop approaches.

Kianzad et al. [13] use a ballpoint drive to assist users in sketching. They employ a proportional-derivative (PD) control loop, which allows users to deviate from the target to a certain extend. We show in our experiments that our optimization scheme outperforms such existing closed-loop approaches. Muscle-Plotter [21] proposes active guidance for users based on electrical muscle stimulation. Their control strategy is based on heuristics for users to share control with the system. Our approach could be applied to their work if the electromagnetic force model is replaced by a model of the interaction between the muscle stimulation and the force users produce.

Magnetic Actuation

Providing magnetically-driven haptic feedback on tabletops is desirable as the force can be exerted through the surface without affecting the display. A common approach is using arrays of controllable electromagnets, combined with permanent magnets embedded in objects on the surface. McIntosh et al. [22] show how a permanent magnet attached to a finger can be used for tracking and haptic feedback for mobile interactions. Fingerflux by Weiss et al. [37] provide near-surface haptic feedback before the finger touches the screen to guide users to appropriate screen locations. Pangaro et al. [28] model the force-field of each electromagnet and combine these using standard aliasing techniques, allowing directed movement of multiple objects on the surface. Similarly, Yoshida et al. [40] use linear induction motors to control objects on a tabletop. Strasnick et al. [34] use electromagnets to control an object on a mobile phone case. Suzuki et al. [35] combine these two works and use a grid of electromagnetic cores to move objects on a tabletop. While our optimization scheme could be applied to such devices as well, smooth motion is problematic due to the low resolution of the grid, and the interaction of forces between multiple electromagnets. Furthermore, magnets are modeled using a simplification of the magnetic pole model (known as Gilbert model), considering only attraction between single point poles, leading to undesirable snapping behavior.

Online Path Following

Optimal reference following given real world influences is studied in depth in the control theory literature. Methods like Model Predictive Control (MPC) [8] optimize the reference path and the actuator inputs simultaneously based on the system state. MPC is widely applied in many robotics (e. g. to control quadrocopters, Mueller et al. [24]) and graphics applications (e. g. for human motion prediction, Da Silva et al. [6]). However, Aguiar et al. [2] show that the tracking error for following timed-trajectories can be larger than if following a geometric path only.

To address this issue, Lam et al. propose Model Predictive Contouring Control (MPCC) [17] to follow a time-free reference, optimizing system control inputs for time-optimal progress. MPCC has been successfully applied in industrial contouring [17], RC racing [20] and in drone cinematography [26]. We also pose our optimization problem in this well established framework. However, to the best of our knowledge, we are the first to apply it for haptic guidance systems where one has to consider both a controllable (i. e. the electromagnetic force) and non-controllable (i. e. the user) system. We contribute a formulation of the problem including models and control algorithms to enable employing MPCC in this context.

OPTIMAL CONTROL FOR EM HAPTIC GUIDANCE

The goal of our online optimal control scheme is to allow users to maintain control and agency over the input device (e. g. pen, stylus), while experiencing dynamic guidance from the system. Importantly, it leverages *time-free references* and thus the dynamics are entirely driven by the pen position over time, which is different from approaches such as MPC.

Overview

The proposed optimization scheme allows us to adjust the magnet position and strength such that it gently pulls the pen tip towards a desired stroke, while allowing users to draw at their desired speed and without fully taking over control. The algorithm is generally hardware agnostic and works for devices with electromagnetic actuators underneath an interaction surface. This can be implemented via bi-axial linear stage as in our prototype (see Figure 2) or via a matrix of electromagnets which would lend itself better towards miniaturization. Furthermore, the algorithm requires a reference trajectory over the optimization horizon. This can be defined a-priori, such as a known shape to be traced, or may be provided dynamically, e. g. the output of a predictive model (e. g. Aksan et al. [3]).

At each time step, we minimize a cost functional over a receding time horizon to find optimized values for system states $\mathbf{x}$ and inputs $\mathbf{u}$. As a high-level abstraction, the cost function

$$\underset{\mathbf{x},\mathbf{u}}{\text{minimize}} \sum \underbrace{C_{\text{force}}(\mathbf{x},\mathbf{u})}_{\text{Eq. 3, 4 \& 5}} + \underbrace{C_{\text{path}}(\mathbf{x},\mathbf{u})}_{\text{Eq. 6}} + \underbrace{C_{\text{progress}}(\mathbf{x},\mathbf{u})}_{\text{Eq. 7}}, \quad (1)$$

serves three main purposes: 1) ensuring that the user perceives haptic feedback of dynamically adjustable force (C_{force}), 2) stays close to the desired path but does not rigidly prescribe it (C_{path}), and 3) makes progress along it (C_{progress}) but allows the user to vary drawing speed freely.

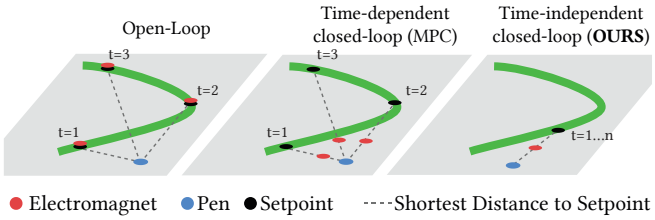

Figure 3. Overview of different control strategies on a target trajectory (*green*), with constant pen position. For open-loop, the position of the electromagnet is identical to the constantly advancing setpoint, leading to loss of haptic guidance. For MPC, although the pen is static, the guidance changes at every timestep since the setpoint advances. In our approach, the setpoint is also based on the pen position, therefore remains stationary in this case and guides the user towards the target trajectory.

CLOSED-LOOP CONTROL

Our main contributions are models and a control strategy that enables using the MPCC framework [17] for electromagnetic haptic guidance. MPCC is a closed-loop *time-independent* control strategy that minimizes a cost function over a fixed receding horizon. There are several advantages in using our formulation over open-loop (as used in dePENd [39]) or time-dependent strategies (e. g. MPC). First, closed-loop control allows to react to user-input, whereas open-loop control removes all user agency. Both MPC and MPCC are closed-loop control strategies. However, MPC tracks a timed reference, requiring a fixed velocity by users. MPCC follows a time-free trajectory, which allows the user to progress at their own speed. Figure 3 illustrates the expected behavior for the different strategies, given that the user slows down or stops moving the pen. The desired behavior here would be that the algorithm essentially "waits", i. e. provides guidances towards a slowly or no-longer advancing setpoint. In this situation, open-loop approaches would lead to lost haptic guidance. Closed-loop time-dependent approaches would guide the pen towards a constantly advancing setpoint (although users do no longer move), which can lead to problems such as the user being guided backwards (e. g. timestep $t = 3$ is in front of $t = 2$).

Our method is designed to exert a force $\mathbf{F}_\theta$ of desired strength onto the pen to guide the user towards the target trajectory $\mathbf{s}$. The path $\mathbf{s}$ of length L is parametrized by $\theta \in [0, L]$. Note that we do not prescribe how fast users draw and hence for each given pen position $\mathbf{p_p}$ we first need to establish the closest position on the path parameterized by $\mathbf{s}(\theta)$. The vector between the pen position and $\mathbf{s}(\theta)$ is defined as $\mathbf{r}_\theta$. We leverage a receding horizon optimization strategy and the global reference can hence be adjusted or replaced entirely at every iteration. The path $\mathbf{s}$ is then a local fit to the global reference. Furthermore,

Table 1. Overview control parameters and values

Name	Range / Value	Description
$\mathbf{p_p}$	$\mathbb{R}^2$	Position of pen
$\mathbf{p_m}$	$\mathbb{R}^2$	Position of electromagnet
$\mathbf{F_a}$	$\mathbb{R}^3$	Electromagnetic force vector
α	$[0, 1]$	Electromagnetic intensity
$\mathbf{s}$	$\theta \in [0, L]$	Target trajectory of length L
$\mathbf{x}$	$[\mathbf{p}_m, \dot{\mathbf{p}}_m, \alpha, \theta]$	System states
$\mathbf{u}$	$[\ddot{\mathbf{p}}_m, \dot{\alpha}, \dot{\theta}]$	System inputs

we seek to find optimized values for the electromagnet intensity α and the in-plane electromagnet position $\mathbf{p}_m$. Solving the error functional given in Eq. (10) at each timestep yields optimized values for system states $\mathbf{x}$ and inputs $\mathbf{u}$.

As common in MPC(C), the system is initialized from measurements at $t = 0$. The system state is then propagated over the horizon with the dynamics model $f(\mathbf{x}, \mathbf{u})$. The system state vector $\mathbf{x}$ contains variables that are controlled by the algorithm (magnet intensity and position, current path progress). The first of the optimized inputs (u_0) is then applied to the physical system, transitioning the system state to x_1, before iteratively repeating the process to allow for correcting modeling errors.

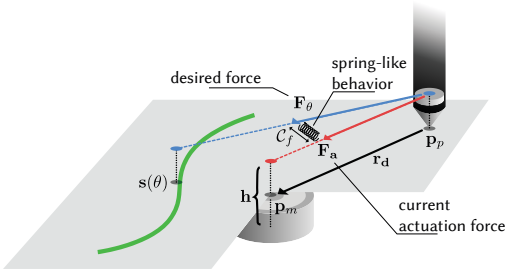

Figure 4. Illustration of actuation force $\mathbf{F_a}$, desired force $\mathbf{F}_\theta$, and the force cost-term C_f associate with the difference between those two forces.

Haptics model: controlling the force of the electromagnet

The main goals of our approach is that users can move freely in terms of position and speed, and that the actuator continuously pulls them towards an advancing setpoint $\mathbf{s}(\theta)$ on the target trajectory $\mathbf{s}$. At any time, the magnet exhibits an actuation force $\mathbf{F_a}$ on the pen, given by our electromagnetic force model (see Implementation section). Therein lies the challenge, illustrated in Figure 4. The setpoint is continuously advancing based on the movement of the pen to ensure progress. The actuator needs to pull the pen towards the setpoint by exhibiting force $\mathbf{F}_\theta$, but currently exhibits $\mathbf{F_a}$. The two forces only align if the pen is exactly at the setpoint, which is rarely the case. To overcome this challenge, we propose modeling this interaction by a spring-like behavior that "pulls" $\mathbf{F_a}$ towards $\mathbf{F}_\theta$. In this way, the magnet continuously guides the pen towards the setpoint, and the force linearly increases with distance between the pen and the target setpoint denoted as:

$$\mathbf{F}_\theta(\mathbf{r}_\theta) = c\ F_0\ \mathbf{r}_\theta\ \mathbf{e}_{\mathbf{r}_\theta}\ . \tag{2}$$

Here $\mathbf{e}_{\mathbf{r}_\theta}$ is a unit vector in the direction of $\mathbf{r}_\theta$, c is a scalar that regulates the stiffness of the spring (in our case $c = 5/h$), F_0 a scaling of the EM force (i. e. the force felt by users) and h the distance between dipoles in z (see Fig. 4). Although simple, this formulation ensures that the haptic guidance is strong under large deviation from the path while vanishing as the user approaches the target path ($r_\theta \to 0$). Note that Eq. 2 is a design choice. Different formulations can be used to achieve different user experiences. Furthermore, replacing our hardware prototype and force-model would allow for adaptation of the remainder of the method to different actuation principles.

The above haptics model serves as basis for our problem formulation of electromagnetic guidance in the MPCC framework. Using the vectors of the current actuation force $\mathbf{F_a}$ and

desired force $\mathbf{F}_\theta$, we formulate a quadratic cost term to penalize the difference between desired force and actual force as:

$$C_f(\mathbf{p_m}, \mathbf{p_p}, \alpha) = \| \mathbf{F}_\theta(\mathbf{r}_\theta) - \mathbf{F_a}(\mathbf{d}) \|^2. \tag{3}$$

where $\mathbf{d}$ is the in-plane vector between the magnet and the pen. Since the actuation force $\mathbf{F_a}$ declines rapidly with distance $\mathbf{d}$, the gradient of C_f goes to 0 for large values of $\mathbf{d}$ causing the optimization to become unstable. To counterbalance this issue we encourage the electromagnet to stay close to the pen:

$$C_d(\mathbf{p_m}, \mathbf{p_p}) = d^2. \tag{4}$$

Finally, we prioritize proximity between the magnet and the pen rather than increasing its force by penalizing excessive use of magnetic intensity α:

$$C_\alpha(\alpha) = \alpha^2. \tag{5}$$

Controlling the position of the electromagnet

We continuously optimize the position of the electromagnet with the goal of keeping the distance between the desired path and the pen minimal. To give the user freedom in deciding their drawing speed we first need to find the reference point $\mathbf{s}(\theta)$ on the target trajectory $\mathbf{s}$. Finding the closest point on the path is an optimization problem itself and hence can not be used within our optimization. Similar to recent work in robot trajectory generation [26, 11], we decompose the distance to the closest point into a contouring and lag error, as shown in Figure 5. $\mathbf{r}_\theta$ is the vector between the pen $\mathbf{p_p}$ and a point $\mathbf{s}(\theta)$ on the spline, and $\mathbf{n}$ as the normalized tangent vector to the spline at that point, which is defined as $\mathbf{n} = \frac{\partial \mathbf{s}(\theta)}{\partial \theta}$. The vector $\mathbf{r}_\theta$ can now be decomposed into a lag error and a contour error (Figure 5). The lag-error C_l is computed as the projection of $\mathbf{r}_\theta$. The contour-error C_c is the component of $\mathbf{r}_\theta$ orthogonal to the normal:

$$\begin{aligned} C_l(\mathbf{p_p}, \theta) &= \|\langle \mathbf{r}_\theta, \mathbf{n} \rangle\|^2, \\ C_c(\mathbf{p_p}, \theta) &= \|\mathbf{r}_\theta - (\langle \mathbf{r}_\theta, \mathbf{n} \rangle)\, \mathbf{n}\|^2. \end{aligned} \tag{6}$$

Separating lag from contouring error allows us, for example, to differentiate how we penalize a deviation from the path (C_c), versus encouraging the user to progress (C_l). We furthermore include cost terms to ensure that the magnet stays ahead of the pen (C_θ) and to encourage smooth progress ($C_{\dot\theta}$) computed as

$$\begin{aligned} C_\theta(\theta) &= -\theta, \\ C_{\dot\theta}(\dot\theta) &= (\dot\theta_t - \dot\theta_{t-1})^2. \end{aligned} \tag{7}$$

Dynamics model

To phrase electromagnetic haptic guidance in the MPCC framework, we contribute a a dynamics model $f(\mathbf{x}, \mathbf{u})$ describing the system dynamics given its states $\mathbf{x}$ and inputs $\mathbf{u}$.

$$\begin{aligned} \dot{\mathbf{x}} &= f(\mathbf{x}, \mathbf{u}) \text{ with} \\ \mathbf{x} = [\mathbf{p}_m, \dot{\mathbf{p}}_m, \alpha, \theta] \in \mathbb{R}^6 &\text{ and } \mathbf{u} = [\ddot{\mathbf{p}}_m, \dot\alpha, \dot\theta] \in \mathbb{R}^4. \end{aligned} \tag{8}$$

The system state $\mathbf{x}$ consists of the position of the electromagnet $\mathbf{p}_m \in \mathbb{R}^2$ and its velocity $\dot{\mathbf{p}}_m$, the magnet intensity α and the current path progress θ. The inputs to the system $\mathbf{u}$ consist of

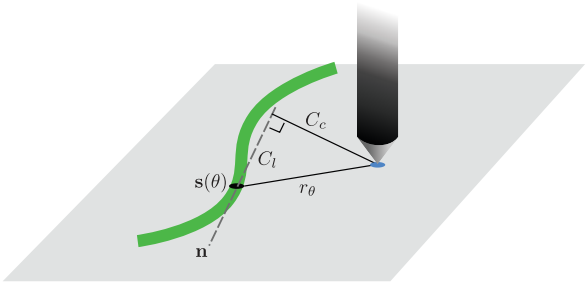

Figure 5. Illustration of lag- and contouring error decomposition.

the in-plane electromagnet accelerations $\ddot{\mathbf{p}}_m$, and velocities $\dot\alpha$ and $\dot\theta$ for magnet intensity and the spline progress respectively. Note that we empirically found that magnet accelerations yield smoother motion than using velocities. The system model is given by the non-linear ordinary differential equations using first and second derivatives as inputs:

$$\ddot{\mathbf{p}}_m = v_m, \quad \dot\alpha = v_\alpha \quad \text{and} \quad \dot\theta = v_\theta, \tag{9}$$

where $v_{(\cdot)}$ are the external inputs. The continuous dynamics model $\dot{\mathbf{x}} = f(\mathbf{x}, \mathbf{u})$ is discretized using a standard forward Euler approach: $\mathbf{x}_{t+1} = f(\mathbf{x}_t, \mathbf{u}_t)$ [12].

In our hardware implementation, we derive the sets of admissible states $\boldsymbol{\chi}$ and inputs $\boldsymbol{\zeta}$ empirically to conform to the physical hardware constraints of the linear stage (e. g. max x,y-position) and EM specifications (e. g. max voltage). These are used in the constrained optimization problem solved in Eq. 11. The pen position is propagated via a standard linear Kalman filter [12]. While not an accurate user model, it works well in practice since the states are recalculated at every timestep.

Term	Description of cost	Eq.
C_f	Decreases difference in magnetic force	3
C_d	Decreases distance between magnet and pen	4
C_α	Encourages close distance over large force	5
C_l	Decreases lag to path contour	6
C_c	Decreases distance to path contour	6
C_θ	Magnet stays ahead of pen	7
$C_{\dot\theta}$	Ensures smooth progress	7

Table 2. Summary of costs terms used in optimization.

Optimization

We combine the cost terms (Table 2) to control the force and position of the actuator to form the final stage cost:

$$\begin{aligned} J_k = \; & w_f C_f(\mathbf{p}_{m,k}, \mathbf{p}_{p,k}, \alpha_k, \theta_k) + \\ & w_d C_d(\mathbf{p}_{m,k}, \mathbf{p}_{p,k}) + w_\alpha C_\alpha(\alpha_k) + \\ & w_l C_l(\mathbf{p}_{p,k}, \theta_k) + w_c C_c(\mathbf{p}_{p,k}, \theta_k) + \\ & w_\theta C_\theta(\theta_k) + w_{\dot\theta} C_{\dot\theta}(\dot\theta_k), \end{aligned} \tag{10}$$

where the scalar weights $w_l, w_c, w_\theta, w_{\dot\theta}, w_f, w_d, w_\alpha > 0$ control the influence of the different cost terms. The values used in our experiments and applications can be found in the Implementation section. The system states and inputs are computed by solving the N-step finite horizon constrained non-linear optimization problem at time instance t.

The final objective therefore is:

$$\underset{\mathbf{x},\mathbf{u},\theta}{\text{minimize}} \quad \sum_{k=0}^{N} w_k \left(J_k + \mathbf{u}_k^T \mathbf{R} \mathbf{u}_\mathbf{k} \right) \tag{11}$$

$$\begin{aligned}
\text{Subject to:} \quad & \mathbf{x}_{k+1} = f(\mathbf{x_k}, \mathbf{u_k}) && \text{(System Model)} \\
& \mathbf{x}_0 = \hat{\mathbf{x}}(t) && \text{(Initial State)} \\
& \theta_0 = \hat{\theta}(t) && \text{(Initial Progress)} \\
& \theta_{k+1} = \theta_k + \dot{\theta}_k dt && \text{(Progress along path)} \\
& 0 \leq \theta_k \leq L && \text{(Path Length)} \\
& \mathbf{x}_k \in \boldsymbol{\chi} && \text{(State Constraints)} \\
& \mathbf{u}_k \in \boldsymbol{\zeta} && \text{(Input Constraints)}
\end{aligned}$$

Here k indicates the horizon stage and the additional weight w_k reduces over the horizon, so that the current timestep has more importance than later timesteps. $\mathbf{R} \in \mathbb{S}_+^{n_u}$ is a positive definite penalty matrix avoiding excessive use of the control inputs. In our implementation we use a horizon length of $N = 10$. Experimentally we found that this is sufficient to yield robust solutions to problem instances and longer horizons did not improve results, yet linearly increases computation time. The algorithm is summarized in Appendix A Alg. 1.

IMPLEMENTATION

In this section, we detail our electromagnetic force model used in our optimal control scheme as well as the implementation of our hardware prototype.

Electromagnetic force model

Our approach requires a model of the interaction between a variable-strength electromagnet (EM) and the permanent magnet in the stylus that is sufficiently accurate and can be evaluated in real time. Accurately modeling the non-linear EM field of the electromagnet's core is typically done through finite element analysis (FEA), which cannot be performed in real time. Similarly, precomputing the volumetric map of the EM field $\mathbf{B_m}$ via FEA for all levels of electrical current is not computationally feasible. We therefore contribute a novel fast approximate yet accurate electromagnetic model that provides a good balance between speed and accuracy to enable haptic guidance in applications such as writing or sketching.

In general, we aim at finding the actuation force on the pen $\mathbf{F_p}$, which is given by integrating over the volume of the permanent magnet in the pen:

$$\mathbf{F_p} = \iiint \nabla \left(\mathbf{M_p} \cdot \mathbf{B_m}(\cdot) \right) dxdydz, \tag{12}$$

where $\mathbf{M_p}$ is the magnetization of pen magnet and $\mathbf{B_m}(\cdot)$ is the EM field evaluated at the pen position, which is too costly to evaluate in real time. Our model approximates this underlying physical phenomena, can be efficiently evaluated at every iteration of our optimization procedure and provides a very good fit to empirical data. In this section, we briefly discuss the most important aspects of our model, for a full derivation and analysis we refer readers to the Appendix B.

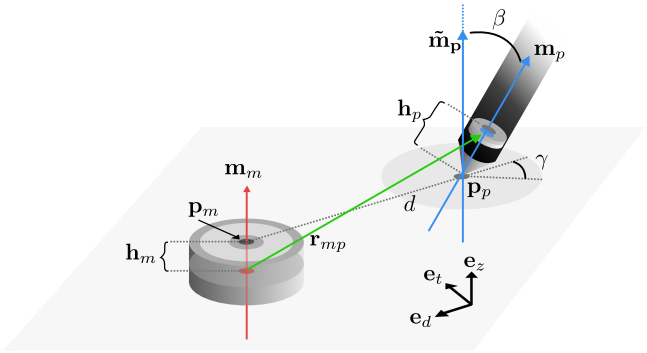

Figure 6. Illustration of the model to compute the force $\mathbf{F_p}$ on dipole $\mathbf{m_p}$ due to dipole $\mathbf{m_m}$.

We make the following two assumptions in our derivation: 1) the electromagnet and the permanent magnet can be approximated as dipoles (i. e. oriented point magnets), and 2) for the smaller dipole (the permanent magnet in the pen) the out-of-plane vector component is much larger than the in-plane counterpart. This allows us to use only the vertical component in the calculation of the force.

The first assumptions allows us to use the standard model by Yung et al. [41] to compute the force exerted by the electromagnet $\mathbf{m_m}$ onto the pen $\mathbf{m_p}$ (see Figure 6) as:

$$\begin{aligned}
\mathbf{F_p} = \frac{3\mu_0}{4\pi r_{mp}^5} \Big[& \left(\langle \mathbf{m_p}, \mathbf{r_{mp}} \rangle \right) \mathbf{m_m} + \left(\langle \mathbf{m_m}, \mathbf{r_{mp}} \rangle \right) \mathbf{m_p} + \\
& \left(\langle \mathbf{m_p}, \mathbf{m_m} \rangle \right) \mathbf{r_{mp}} - \frac{5 \left(\langle \mathbf{m_p}, \mathbf{r_{mp}} \rangle \right) \left(\langle \mathbf{m_m}, \mathbf{r_{mp}} \rangle \right)}{r_{mp}^2} \mathbf{r_{mp}} \Big],
\end{aligned} \tag{13}$$

where μ_0 is a constant (vacuum permeability $4\pi\ 10^{-7}$ [H/m]) and $\mathbf{r_{mp}}$ is the 3D vector between the centers of the electromagnet and pen dipoles. In contrast to FEA, this expression is analytic and differentiable, thus suited for iterative optimization. Figure 6 shows all quantities needed to compute the total magnetic force exerted on the pen. The expression does, however, lead to an actuation force $\mathbf{F_p}$ that depends on the tilt of the pen. In pre-tests, we found that users can not perceive a difference in strength when tilting the pen in-place. We therefore leverage our second assumption, which reduces the EM model from 6 DOF to 3 DOF, to avoid this computation.

Based on the second assumption, we can retrieve the two vertical force vectors of the electromagnet $\mathbf{m_m}$ and the pen $\tilde{\mathbf{m}}_\mathbf{p}$. The vector between the two centers can now be computed as $\mathbf{r_{mp}}$. We then project this vector onto the plane, yielding the final vector d between the pen tip and the in-plane projection of the actuator dipole. The total force acting on the pen (Eq. 13) can now be decomposed as:

$$\mathbf{F_p} = F_a\ \mathbf{e_d} + F_z\ \mathbf{e_z}\ . \tag{14}$$

Here $\mathbf{F_a} = F_a\ \mathbf{e_d}$ represents the in-plane quantity we seek to control, as it is the magnitude F_a of the force vector $\mathbf{F_a}$ in the direction of a unit vector $\mathbf{e_d}$ along d. F_z is the vertical force components which pulls the pen downwards. During our experiments there was no significant change in perceived

friction when comparing the drawings with and without electromagnet (i. e. with or without F_z). For this reason we do not actively account for F_z in our optimization and only maintain the in-plane force contribution ($\mathbf{e_d}$ direction). The actuation force as function of pen-magnet separation is obtained as:

$$\mathbf{F_a} = \alpha\, F_0 \left(\frac{d\left(4 - \frac{d^2}{h^2}\right)}{h\left(1 + \frac{d^2}{h^2}\right)^{\frac{7}{2}}} \right) \mathbf{e_d}, \tag{15}$$

where $\alpha \in [0, 1]$ is a dimensionless scalar to control the desired strength of the force that should be felt by users, h is the center-to-center distance between both magnets projected on to the z-axis (Figure 4) and F_0 is a constant force parameter given by the expression,

$$F_0 = \frac{3\,\mu_0\, m_p\, m_m}{4\,\pi\, h^4}\,. \tag{16}$$

The actuation force F_a is zero if the two magnets are aligned with one another ($d = 0$), it has a maximum $F_a^{max} = 0.9\, F_0$ at $d = 0.39h$, and we can assume there is no more attraction for distances $d > 2h$. Note that the second assumption (only use in-plane component) lead only to a small approximation error Compared to an angle dependent formulation (see Appendix B.2), a tilt of up to $\beta = 30°$ leads to a max error in our model (Equation 30) equivalent to shifting the distance d by ± 3 mm. This uncertainty in d is comparable with the in-plane positioning error (dispersion) of our hardware prototype. An angle dependent formulation of our model (i. e. 6 DOF) can be found in Appendix B.2 for future use in cases where the pen angle is tracked. This model remains valid for other hardware implementations involving a single moving electromagnet or can be easily extended onto a grid of fix electromagnets.

Hardware prototype

We have developed one possible hardware instance that utilizes our optimization scheme for an in-plane haptic guidance system (see Figure 2). Our system consists of 3 main components: 1) a moving platform that controls the 2D location of the electromagnetic actuator, 2) an input device such as a stylus, and 3) an output device such as a digital tablet or digitizer used in combination with a non-digital drawing surface.

Motion platform

The motion platform consists of a controllable electromagnet on a bi-axial linear stage directly underneath the drawing plane. The linear stage has two orthogonal 12 mm lead screws, which are driven by two 24 V, 4.0 A NEMA23 high-torque stepper motors. We control the motors with a DQ542MA stepper driver and an Arduino UNO. As electromagnet, we use an Intertec ITS-MS-5030-12VDC magnet (5 cm diameter, 3 cm height, 12 V), controlled via pulse-width modulation. It can deliver up to 488 mN of lateral force at 11 W. We used FEM analysis to select this magnet from a range of commercially available magnets [5]. It provides a balance between power consumption, size, and force, i. e. it delivers a strong perceivable force while having a small footprint relative to our hardware.

To measure the positional dispersion of the motion platform, we moved the electromagnet at full strength ($\alpha = 1$) to 300 random locations and then always back to the center of the drawing surface. During theses trials, a user held the pen upright and followed the magnet passively. By measuring the difference in target and actual position, we found that our system yields 2.8 mm (± 0.8 mm) of point dispersion. We believe this is sufficient for most applications and our experiments. One of the factors that contribute to this dispersion is the vanishing of the actuation force F_a as $d \to 0$. This can lead to the pen motion stopping slightly before it reaches the target.

Software

Our software runs on a standard PC (Intel Core i7-4770 CPU 4 cores at 3.40 GHz) in all our experiments. The solver is implemented in FORCES Pro [7], which produces efficient C-code. The following weight values are used for our control scheme (Equation 10):

w_l	w_c	w_θ	$w_{\dot\theta}$	w_f	w_d	w_α	w_v	w_m
1.5	1.5	10.	0.1	10.	0.05	7.	1.	1.

Due to the steepness of the electromagnetic force $\mathbf{F_p}$ and the potentially fast pen motion, runtime and latency are crucial performance metrics. The optimization algorithm contributes to both, whereas latency is dominated by the hardware and I/O. The mean solve time for a problem instance is 7.4 ms (± 3.0 ms). This can be expected to be mostly constant since we do not manipulate the system state space and the only measured input comes from the pen. The hardware and overall system latency adds to the solve time. We use a high-speed camera (1000 fps) to establish the motion (pen) to motion (magnet) latency. This yields an approximate latency of ~10 ms. Given the combined latency envelope of ~20 ms, we did not experience any abrupt pen snapping in our experiments.

Input and Output Devices

Our primary input and output devices for our user experiments consist of a 3D printed ballpoint pen with a permanent ring magnet mounted in the shaft (see Figure 2) and a piece of paper. The strokes are recorded by a Sensel Morph pressure sensitive touch pad [23]. If the system cannot locate the pen (e. g. when it is lifted) the last known position is used. We chose the Sensel for its high spatial resolution (6502 DPI), high speed (500 Hz) and low latency (2 ms), according to specification, and since the sketching surface does not interfere with the input recognition. Additionally, we developed an all digital input/output system with a multi-touch tablet + stylus. We use a Galaxy Tab A tablet with capacitive input and an off-the-shelf stylus with a permanent magnet placed near the tip. This magnet is slightly bigger (12 mm radius, 12 mm height) to compensate for the increase in tablet thickness.

EVALUATION

We first evaluated if our optimization scheme is beneficial for users in providing haptic guidance compared to a no-feedback baseline. In a second experiment, we compared our method with an open-loop and a closed-loop approach.

Experiment 1 - Haptic feedback

We compared our MPCC formulation with a no-feedback baseline to gather insights on task performance and user perception.

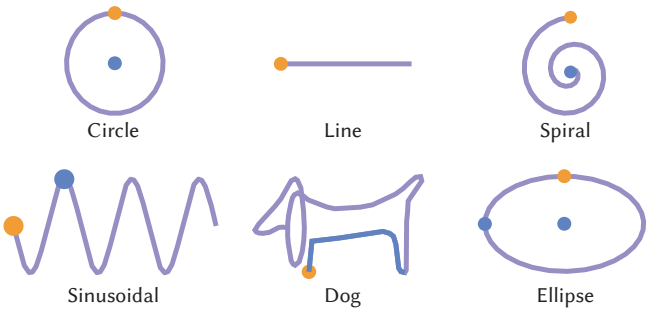

Figure 7. Shapes of our user tests. The drawing surface only contained sparse visual references (shown in blue) and starting positions (orange).

Users were asked to draw several shapes (see Figure 7) and we evaluated accuracy and subjective feedback.

Procedure and tasks

We recruited 12 participants from the local university, all without professional drawing experience. Users were given an introduction to the system functionality and got to experience the system in a self-timed training phase. During the experiment we asked each participant to draw six basic shapes, each with and without haptic feedback. The presentation order of shapes and interface condition was counterbalanced. The drawing surface (white piece of paper) only contained a starting point and, in the case of more complex shapes, limited additional visual guidance (see Figure 7). Furthermore, the participants were shown a scaled version during task execution (scaled to prevent 1:1 copying). After the full experiment, users completed a questionnaire on their preference.

Quantitative Results

We compute the Hausdorff-like distance [30] between the drawn path and the reference path as error metric. To make the metric robust to drawing speed, we re-sample both paths equidistantly. To ensure fairness we also compute the inverse distance (reference to drawn path). A Kolmogorov-Smirnov test [15] indicated that the set of uni-directional distances is not significantly different from the set of inverse distances. We therefore only report uni-directional distances. The quantitative results for each target averaged over all participants are summarized in Table 3. Our method on average resulted in a 66% (± 24.5%) lower error, i. e. it improve the average point-to-path difference by 1.54 mm. A two-way ANOVA on the mean error revealed a main effect for the feedback type ($F=46.187$, $p<.001$) and for the shapes ($F=11.771$, $p < .001$). Post-hoc analysis revealed that the line was statistically significantly different from all other shapes. This indicates that our method is beneficial for non-trivial shapes.

Qualitative Results

A brief exit interview shows that users subjectively rate the system favorably, on a 5-point Likert scale (5 is best), in terms of accuracy (4.33 ± 0.62), speed (4.00 ± 0.91), force (3.50 ± 0.86) and overall performance (4.50 ± 0.9). While we acknowledge that this might be in part due to novelty effects, we believe that the quantitative results indicate that our system is beneficial for users in general. The ratings indicate that participants generally see benefit in our approach and are not disturbed or hindered when using our approach.

Table 3. Mean accuracy (*mm*). * indicates statistical significance (α.05).

	With		Without		
Scenario	Mean	SD	Mean	SD	Err %
Circle*	**2.19**	0.90	4.26	2.39	0.51
Line	1.18	0.80	**1.03**	0.84	1.15
Spiral*	**2.55**	0.75	4.38	1.64	0.58
Sinus*	**2.53**	0.70	5.08	2.19	0.50
Dog*	**2.31**	0.54	3.81	1.32	0.60
Ellipse*	**2.40**	0.56	3.84	1.22	0.62

Experiment 2: Comparison of control strategies

In this second experiment, we compared our time-free closed-loop optimization strategy to a simpler MPC variant and our implementation of dePENd [39], denoted as dePENd*.

Procedure and tasks

We asked twelve new participants (students and staff from a local university) to draw one complex shape (dog in Figure 7) in three different conditions: *dePENd** , time-dependent closed loop (*MPC*), and time-free closed loop (*Ours*), counterbalanced using a latin square. The speed of the system in the time-dependent cases was decided empirically based on pretests to work well at regular drawing speeds. After receiving instructions and a brief training, participants completed the three drawings. Participants were also encouraged to provide comments during the individual conditions.

Data collection

We analyze three measures: 1) the mean distance from the pen to the path, 2) the mean distance from the pen position projected onto the path and the setpoint along the path, denoted as $d(pen, \mathbf{s}(\theta))$, and 3) the mean distance from the pen to the electromagnet. By taking the mean of the error terms over subjects we ensured equal numbers of datapoints, accounting for differences in speed. Participants were instructed to draw at roughly constant speed. This was done to ensure fairness in comparing our approach with the open-loop approach, which would deteriorate if the variability of the drawing speed were to high. Note that our approach does generally not require this assumption.

Quantitative results

Table 4 summarizes our quantitative findings. Not surprisingly, the distance from the electromagnet to the pen and $d(pen, \mathbf{s}(\theta))$ for *dePENd** is quite large. Since the force exerted on the pen falls-off quadratically with distance, participants often lost any haptic guidance early on, confirmed via user comments such as "I don't feel anything" (P3) and "Is the system on?" (P6).

A Kruskal-Wallis test revealed that our approach has the highest accuracy compared to *dePENd** and MPC ($H(2)=20.76$, $p<.001$). Furthermore, the setpoint $\mathbf{s}(\theta)$ ($H(2)=7.362$, $p<.05$)

Table 4. Mean distances in *mm* for Experiment 2).

	|pen-path|	d(pen, $s(\theta)$)	|pen-em|
*dePENd**	4.1(±0.7)	38.0(±56.9)	38.2(±25.1)
MPC	3.9(±1.3)	45.0(±50.8)	8.6(±1.6)
Ours	**2.0**(±0.6)	**6.2**(±0.8)	**4.6**(±0.9)

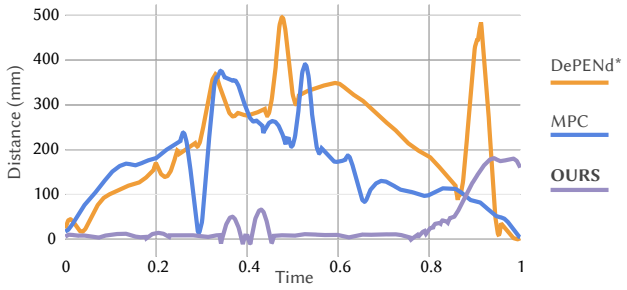

Figure 8. Comparison of error (path distance pen-s(θ)) over time for a single participant (P1). The inverse u-shape illustrates that the setpoint s(θ) moves at a different speed than the user for *dePENd and MPC. The data is smoothed to increase readability.**

and the electromagnet ($H(2)=27.12$, $p < .001$) are closest to the pen using our approach. Thus our time-free formulation overcomes both problems of wrong setpoints (*MPC*) and a run-away electromagnet (*dePENd**). Figure 8 shows one typical example of a user. Both the distance along the path and the pen-magnet distance fluctuate strongly for *dePENd** and *MPC* control strategies. Our approach yielded a continuously low error.

While *MPC* reduces the distance from the pen to the magnet, it does not optimize for the progress along the path and hence may pull the pen into undesired directions. Furthermore, we saw that *MPC* produced extreme corner cutting behavior to catch up to the advancing setpoint. Both *dePENd** and *MPC* also produce results with high standard deviations. This is likely due to the absence of direct coupling between user feedback and path progress, which makes it possible for the user to lag behind the setpoint significantly (albeit at the cost of reduced force feedback). In our approach, the path progress is adjusted to the user's drawing speed, drastically reducing the standard deviation and in consequence ensuring delivery of force feedback throughout the drawn path.

Qualitative results

From our observations we saw that $\mathbf{s}(\theta)$ was either in front or behind the user for MPC. This was also confirmed in our interview, where people especially commented on the MPC strategy: "The system tries to push me in the wrong direction" (P2) and "It is counteracting me" (P11). In contrast with our formulation the magnet remains always slightly ahead of the pen, resulting in users commenting on our approach as the most preferred condition. In the words of one subject this is: "since I still had control" (P9).

In summary, theses initial results indicate that our approach outperforms existing open-loop and time-dependent closed-loop approaches. *dePENd** causes numerous problems, including users not perceiving any haptic feedback. This is especially troublesome in settings where autonomy is desired. In MPC the haptic feedback is perceived, but can be erroneous. This is especially evident when users do not conform to the expected behavior. We plan to perform more in-depth experiments to investigate, for which applications our approach can be especially beneficial, and for which levels of autonomy.

APPLICATIONS

To further demonstrate the potential of our approach we illustrate possible usage-scenarios including calligraphy, outlining and inking. Finally, we combine the haptic feedback mechanism with a simple digital drawing application to initially explore the possibility of dynamic references.

Calligraphy

Figure 9 illustrates writing of flourished characters, with only minimal visual guidance (single starting point). Our system takes the character as input, users can then draw at their desired speed. Although an offset from the reference path remains, the lines are smooth and the overall shape is close to the desired characters.

Figure 9. Our approach can be used as a guidance system for calligraphy, where users either follow a target path very closely, or deviate if desired.

Outlining & inking

Figure 10 illustrates the effect of two core capabilities of the proposed approach. Here we first outline the proportions of the dragon head (gray guidance lines) and then use different pens to ink-in the details. Note that the system provides haptic guidance but allows the user to draw the shape in different styles (e. g. the ears of the two upper dragons) and with varying high-frequency detail, while maintaining similarity to the reference shape. This is a direct consequence of using time-free closed loop control approach. In this case, all four variants were drawn without changes to the system or desired path.

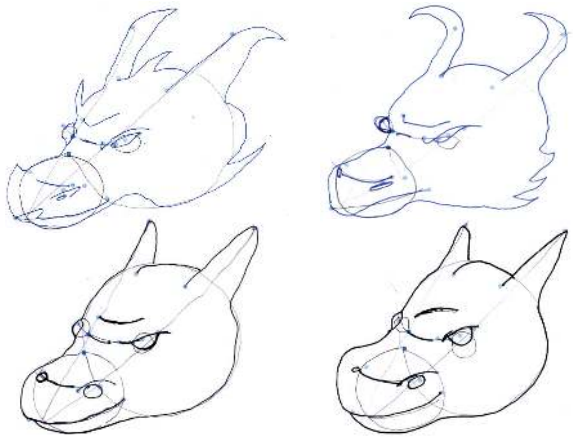

Figure 10. Different variants of the same dragon, drawn with identical system settings by a novice. Each pair of drawings used with different tools. First a pencil for proportions and a fine-liner (top) or pencil (bottom) to ink-in details. Multi-stroke lines are achieved by approaching each separate instance as a new drawing.

Virtual tools

Using a digital tablet with capacitive display (Figure 11) we explore integrating dynamically changing references. In a sketching application, artist select different virtual tools, and position and configure these anywhere. The canvas and the haptic feedback system then pull the stylus towards these virtual guides. In Figure 11, the user has selected a tool that helps them when drawing an ellipse that snaps to a previous part of the drawing, both visually and in terms of haptics.

Figure 11. Virtual tools can be used to dynamically construct a reference path combining haptic and visual feedback. Here a simple drawing application combines freeform sketching with different virtual rules and guides that can be felt by the user.

DISCUSSION

Our experiments indicate that the proposed approach indeed increases accuracy in drawing tasks and that users perceive the system favorably. While our system increased users' accuracy for complex shapes, it did not yield any improvements for the straight line. This may be explained by user feedback, that the maximum speed of the linear stage is a limiting factor in the current implementation. In our interviews, some users indicated that they had the feeling that their drawings without feedback were more accurate once they experienced the haptic guidance. This hints at the possibility of short-term muscle memory when using our haptic guidance approach. Long-term learning is a very interesting area to explore for our approach and haptic guidance systems in general. We plan to conduct such experiments in the future.

Our experiments currently focused on drawing and sketching applications. We believe that our control strategy will be beneficial for a broad set of applications. We started exploring the usage of our approach with a tablet and digital stylus. More experiments, however, are needed to find out at which level of complexity our approach becomes the most beneficial. Allowing users to adjust their input on-demand is crucial for most applications, especially since systems most often do not have complete knowledge of users' target path. Our approach is a first step in the direction of balancing user input and system control for haptic guidance systems, and can be extended to other devices beyond electromagnetic systems if appropriate force models are provided.

In terms of hardware, the speed of the employed linear stage was a limiting factor, without which users would have been able to complete drawings and general inputs faster. We plan to implement advances in that direction in the future. This may include faster and smaller form-factor linear stages or a matrix of stationary electromagnets. The former would require no changes to our formulation, whereas the latter would require changes to the EM model and the dynamics model. An EM matrix opens-up the path towards a thin form-factor design and is a particularly interesting research direction.

Once the hardware-induced speed limitation is overcome, efficient closed-loop control approaches become an interesting direction for future work, since faster pen motion would also tighten the latency and accuracy budget. In the context of sensing it would be interesting to incorporate a mechanism to reconstruct the tilt of the pen. This could be achieved for example via an accelerometer built into the pen or via a grid of hall-sensors underneath the surface. Information on the pen tilt could then be combined with the angle dependent formulation of our EM model (see Appendix C). Furthermore, we believe there are many research opportunities in combining our approach with ink beautification approaches (e. g. [33, 32, 38]). Particularly interesting would be to leverage fully predictive models for non-drawing applications (e. g. DeepWriting [3]).

We believe that it could be an interesting direction for future work to combine our approach with different types of haptic feedback, either environment mounted or body-worn, and different form factors such as spherical electromagnets [18, 42]. Electromagnetic feedback in combination with spatial actuation maybe interesting in other settings. For example, a magnet mounted to a robotic arm could deliver contact-less feedback in VR scenarios. It would also be interesting to investigate how to best exploit the system capabilities in the context of motor memory and learning. All these scenarios make it necessary that a system interactively reacts to user input. Our approach enables such applications, and can generalize to such systems that go beyond 2D haptic guidance systems.

CONCLUSION

We have proposed a novel optimization scheme for electromagnetic haptic guidance systems based on the MPCC framework. Our approach balances user input and system control so that users can adjust their trajectory and speed on-demand. It optimizes the system states and its inputs over a receding horizon via solving a stochastic optimal control problem at each timestep. Our formulation has been designed to provide dynamically adjustable forces and automatically adjusts magnet position and strength. It can be evaluated analytically and is hence suitable for iterative, real-time optimization approaches. We implemented our approach on a prototypical hardware platform and showed experimentally that the feedback is well receive by users, and provides higher accuracy than open-loop and time-dependent closed-loop approaches. We believe that our approach provides a principled way towards haptic guidance where users retain agency while being unobtrusively assisted, and is applicable broadly in applications such as drawing, sketching, writing or guidance via virtual haptic tools.

ACKNOWLEDGEMENTS

This work was supported in part by grants from the Hasler Foundation (Switzerland), ERC (OPTINT StG-2016-717054), the ETH Zurich Postdoctoral Fellowship Programme (ETH/Cofund 18-1 FEL-39), NSF CAREER award 1652515, the NSF grants IIS-1320635, OAC-1835712, OIA-1937043, CHS-1908767, CHS-1901091, a gift from Adobe Research, a gift from nTopology, and a gift from Advanced Micro Devices, Inc.

REFERENCES

[1] David A. Abbink, Mark Mulder, and Erwin R. Boer. 2012. Haptic shared control: smoothly shifting control authority? *Cognition, Technology & Work* 14, 1 (2012), 19–28. DOI: http://dx.doi.org/10.1007/s10111-011-0192-5

[2] A. Pedro Aguiar, Joao P. Hespanha, and Petar V. Kokotovic. 2008. Performance limitations in reference tracking and path following for nonlinear systems. *Automatica* 44, 3 (2008), 598 – 610. DOI: http://dx.doi.org/10.1016/j.automatica.2007.06.030

[3] Emre Aksan, Fabrizio Pece, and Otmar Hilliges. 2018. DeepWriting: Making Digital Ink Editable via Deep Generative Modeling. In *Proceedings of the 2018 CHI Conference on Human Factors in Computing Systems (CHI '18)*. Association for Computing Machinery, New York, NY, USA, 1–14. DOI: http://dx.doi.org/10.1145/3173574.3173779

[4] Karl Johan Åström and Tore Hägglund. 1995. *PID controllers: theory, design, and tuning*. Vol. 2. Instrument society of America Research Triangle Park, NC.

[5] COMSOL Multiphysics. COMSOL Multiphysics. (????). www.comsol.com.

[6] M. Da Silva, Y. Abe, and J. Popović. 2008. Simulation of Human Motion Data using Short-Horizon Model-Predictive Control. *Computer Graphics Forum* 27, 2 (2008), 371–380. DOI: http://dx.doi.org/10.1111/j.1467-8659.2008.01134.x

[7] Alexander Domahidi and Juan Jerez. 2014. FORCES Professional. embotech GmbH (http://embotech.com/FORCES-Pro). (2014).

[8] T. Faulwasser, B. Kern, and R. Findeisen. 2009. Model predictive path-following for constrained nonlinear systems. In *Proceedings of the 48h IEEE Conference on Decision and Control (CDC)*. 8642–8647. DOI: http://dx.doi.org/10.1109/CDC.2009.5399744

[9] Piyum Fernando, Roshan Lalintha Peiris, and Suranga Nanayakkara. 2014. I-Draw: Towards a Freehand Drawing Assistant. In *Proceedings of the 26th Australian Computer-Human Interaction Conference on Designing Futures: The Future of Design (OzCHI '14)*. Association for Computing Machinery, New York, NY, USA, 208–211. DOI: http://dx.doi.org/10.1145/2686612.2686644

[10] Benjamin A. C. Forsyth and Karon E. MacLean. 2006. Predictive Haptic Guidance: Intelligent User Assistance for the Control of Dynamic Tasks. *IEEE Transactions on Visualization and Computer Graphics* 12, 1 (Jan. 2006), 103–113. DOI:http://dx.doi.org/10.1109/TVCG.2006.11

[11] Christoph Gebhardt, Stefan Stevšić, and Otmar Hilliges. 2018. Optimizing for Aesthetically Pleasing Quadrotor Camera Motion. *ACM Trans. Graph.* 37, 4, Article 90 (July 2018), 11 pages. DOI: http://dx.doi.org/10.1145/3197517.3201390

[12] Bruce P Gibbs. 2011. *Advanced Kalman filtering, least-squares and modeling: a practical handbook*. John Wiley & Sons.

[13] Soheil Kianzad, Yuxiang Huang, Robert Xiao, and Karon E. MacLean. 2020. Phasking on Paper: Accessing a Continuum of PHysically Assisted SKetchING. In *Proceedings of the 2020 CHI Conference on Human Factors in Computing Systems (CHI '20)*. Association for Computing Machinery, New York, NY, USA, 1–12. DOI:http://dx.doi.org/10.1145/3313831.3376134

[14] Hyunjung Kim, Seoktae Kim, Boram Lee, Jinhee Pak, Minjung Sohn, Geehyuk Lee, and Woohun Lee. 2008. Digital Rubbing: Playful and Intuitive Interaction Technique for Transferring a Graphic Image onto Paper with Pen-Based Computing. In *CHI '08 Extended Abstracts on Human Factors in Computing Systems (CHI EA '08)*. Association for Computing Machinery, New York, NY, USA, 2337–2342. DOI: http://dx.doi.org/10.1145/1358628.1358680

[15] Andrey Kolmogorov. 1933. Sulla determinazione empirica di una lgge di distribuzione. *Inst. Ital. Attuari, Giorn.* 4 (1933), 83–91.

[16] Denise Lam, Chris Manzie, and Malcolm Good. 2010. Model predictive contouring control. In *Decision and Control (CDC), 2010 49th IEEE Conference on*. IEEE, 6137–6142. DOI: http://dx.doi.org/10.1109/CDC.2010.5717042

[17] Denise Lam, Chris Manzie, and Malcolm C Good. 2013. Model predictive contouring control for biaxial systems. *IEEE Transactions on Control Systems Technology* 21, 2 (2013), 552–559. DOI: http://dx.doi.org/10.1109/TCST.2012.2186299

[18] Thomas Langerak, Juan Zarate, David Lindlbauer, Christian Holz, and Otmar Hilliges. 2020. Omni: Volumetric Sensing and Actuation of Passive Magnetic Tools for Dynamic Haptic Feedback. In *Proceedings of the Annual Symposium on User Interface Software and Technology (UIST '20)*.

[19] Long-Fei Lin, Shan-Yuan Teng, Rong-Hao Liang, and Bing-Yu Chen. 2016. Stylus Assistant: Designing Dynamic Constraints for Facilitating Stylus Inputs on Portable Displays. In *SIGGRAPH ASIA 2016 Emerging Technologies (SA '16)*. Association for Computing Machinery, New York, NY, USA, Article Article 14, 2 pages. DOI:http://dx.doi.org/10.1145/2988240.2988255

[20] Alexander Liniger, Alexander Domahidi, and Manfred Morari. 2014. Optimization-based autonomous racing of 1:43 scale RC cars. *Optimal Control Applications and Methods* (2014). DOI: http://dx.doi.org/10.1002/oca.2123

[21] Pedro Lopes, Doăa Yüksel, François Guimbretière, and Patrick Baudisch. 2016. Muscle-Plotter: An Interactive System Based on Electrical Muscle Stimulation That Produces Spatial Output. In *Proceedings of the 29th*

Annual Symposium on User Interface Software and Technology (UIST '16). Association for Computing Machinery, New York, NY, USA, 207–217. DOI: http://dx.doi.org/10.1145/2984511.2984530

[22] Jess McIntosh, Paul Strohmeier, Jarrod Knibbe, Sebastian Boring, and Kasper Hornbæk. 2019. Magnetips: Combining Fingertip Tracking and Haptic Feedback for Around-Device Interaction. In *Proceedings of the 2019 CHI Conference on Human Factors in Computing Systems (CHI '19)*. Association for Computing Machinery, New York, NY, USA, 1–12. DOI:http://dx.doi.org/10.1145/3290605.3300638

[23] morph. 2017. Sensel Morph Official Site. (2017). https://sensel.com/pages/the-sensel-morph.

[24] M.W. Mueller and R. D'Andrea. 2013. A model predictive controller for quadrocopter state interception. In *Proceedings of the European Control Conference (ECC), 2013*. 1383–1389. DOI: http://dx.doi.org/10.23919/ECC.2013.6669415

[25] James Mullins, Christopher Mawson, and Saeid Nahavandi. 2005. Haptic handwriting aid for training and rehabilitation. In *Systems, Man and Cybernetics, 2005 IEEE International Conference on*, Vol. 3. IEEE, 2690–2694. DOI: http://dx.doi.org/10.1109/ICSMC.2005.1571556

[26] Tobias Nägeli, Lukas Meier, Alexander Domahidi, Javier Alonso-Mora, and Otmar Hilliges. 2017. Real-time Planning for Automated Multi-View Drone Cinematography. *ACM Transactions on Graphics (Proceedings of ACM SIGGRAPH)* (2017).

[27] Ken Nakagaki and Yasuaki Kakehi. 2014. Comp*Pass: A Compass-Based Drawing Interface. In *CHI '14 Extended Abstracts on Human Factors in Computing Systems (CHI EA '14)*. Association for Computing Machinery, New York, NY, USA, 447–450. DOI: http://dx.doi.org/10.1145/2559206.2574766

[28] Gian Pangaro, Dan Maynes-Aminzade, and Hiroshi Ishii. 2002. The Actuated Workbench: Computer-Controlled Actuation in Tabletop Tangible Interfaces. In *Proceedings of the 15th Annual ACM Symposium on User Interface Software and Technology (UIST '02)*. Association for Computing Machinery, New York, NY, USA, 181–190. DOI: http://dx.doi.org/10.1145/571985.572011

[29] Huaishu Peng, Amit Zoran, and François V. Guimbretière. 2015. D-Coil: A Hands-on Approach to Digital 3D Models Design. In *Proceedings of the 33rd Annual ACM Conference on Human Factors in Computing Systems (CHI '15)*. Association for Computing Machinery, New York, NY, USA, 1807–1815. DOI: http://dx.doi.org/10.1145/2702123.2702381

[30] R Tyrrell Rockafellar and Roger J-B Wets. 2009. *Variational analysis*. Vol. 317. Springer Science & Business Media.

[31] Roy Shilkrot, Pattie Maes, and Amit Zoran. 2014. Physical Rendering with a Digital Airbrush. In *ACM SIGGRAPH 2014 Studio (SIGGRAPH '14)*. Association for Computing Machinery, New York, NY, USA, Article Article 40, 1 pages. DOI: http://dx.doi.org/10.1145/2619195.2656328

[32] Edgar Simo-Serra, Satoshi Iizuka, and Hiroshi Ishikawa. 2018. Mastering Sketching: Adversarial Augmentation for Structured Prediction. *ACM Trans. Graph.* 37, 1, Article 11 (Jan. 2018), 13 pages. DOI: http://dx.doi.org/10.1145/3132703

[33] Edgar Simo-Serra, Satoshi Iizuka, Kazuma Sasaki, and Hiroshi Ishikawa. 2016. Learning to Simplify: Fully Convolutional Networks for Rough Sketch Cleanup. *ACM Trans. Graph.* 35, 4, Article 121 (July 2016), 11 pages. DOI:http://dx.doi.org/10.1145/2897824.2925972

[34] Evan Strasnick, Jackie Yang, Kesler Tanner, Alex Olwal, and Sean Follmer. 2017. ShiftIO: Reconfigurable Tactile Elements for Dynamic Affordances and Mobile Interaction. In *Proceedings of the 2017 CHI Conference on Human Factors in Computing Systems (CHI '17)*. Association for Computing Machinery, New York, NY, USA, 5075–5086. DOI: http://dx.doi.org/10.1145/3025453.3025988

[35] Ryo Suzuki, Jun Kato, Mark D. Gross, and Tom Yeh. 2018. Reactile: Programming Swarm User Interfaces through Direct Physical Manipulation. In *Proceedings of the 2018 CHI Conference on Human Factors in Computing Systems (CHI '18)*. Association for Computing Machinery, New York, NY, USA, 1–13. DOI: http://dx.doi.org/10.1145/3173574.3173773

[36] Akiko Teranishi, Georgios Korres, Wanjoo Park, and Mohamad Eid. 2018. Combining full and partial haptic guidance improves handwriting skills development. *IEEE transactions on haptics* 11, 4 (2018), 509–517. DOI:http://dx.doi.org/10.1109/TOH.2018.2851511

[37] Malte Weiss, Chat Wacharamanotham, Simon Voelker, and Jan Borchers. 2011. FingerFlux: Near-Surface Haptic Feedback on Tabletops. In *Proceedings of the 24th Annual ACM Symposium on User Interface Software and Technology (UIST '11)*. Association for Computing Machinery, New York, NY, USA, 615–620. DOI:http://dx.doi.org/10.1145/2047196.2047277

[38] Jun Xing, Li-Yi Wei, Takaaki Shiratori, and Koji Yatani. 2015. Autocomplete Hand-Drawn Animations. *ACM Trans. Graph.* 34, 6, Article 169 (Oct. 2015), 11 pages. DOI:http://dx.doi.org/10.1145/2816795.2818079

[39] Junichi Yamaoka and Yasuaki Kakehi. 2013. DePENd: Augmented Handwriting System Using Ferromagnetism of a Ballpoint Pen. In *Proceedings of the 26th Annual ACM Symposium on User Interface Software and Technology (UIST '13)*. Association for Computing Machinery, New York, NY, USA, 203–210. DOI: http://dx.doi.org/10.1145/2501988.2502017

[40] Shunsuke Yoshida, Haruo Noma, and Kenichi Hosaka. 2006. Proactive desk II: Development of a new multi-object haptic display using a linear induction motor. In *Virtual Reality Conference, 2006*. IEEE, 269–272. DOI:http://dx.doi.org/10.1109/VR.2006.110

[41] Kar W Yung, Peter B Landecker, and Daniel D Villani. 1998. An analytic solution for the force between two magnetic dipoles. *Physical Separation in Science and Engineering* 9, 1 (1998), 39–52.

[42] Juan Zarate, Thomas Langerak, Bernhard Thomaszewski, and Otmar Hilliges. 2020. Contact-free Nonplanar Haptics with a Spherical Electromagnet. In *2020 IEEE Haptics Symposium (HAPTICS)*. 698–704.

[43] Amit Zoran and Joseph A. Paradiso. 2013. FreeD: A Freehand Digital Sculpting Tool. In *Proceedings of the SIGCHI Conference on Human Factors in Computing Systems (CHI '13)*. Association for Computing Machinery, New York, NY, USA, 2613–2616. DOI: http://dx.doi.org/10.1145/2470654.2481361

[44] Amit Zoran, Roy Shilkrot, Pragun Goyal, Pattie Maes, and Joseph A Paradiso. 2014. The wise chisel: The rise of the smart handheld tool. *IEEE Pervasive Computing* 13, 3 (2014), 48–57. DOI: http://dx.doi.org/10.1109/MPRV.2014.59

APPENDIX
CONTROL ALGORITHM

Algorithm 1: Closed Loop Haptic Feedback Control.

Function *MPCC(***x0**, **w**, $\mathbf{p_p}$, **parameters***)*
  $[C_l, C_c, C_\theta, C_{\dot\theta}]$ ←compute lag and contour error
  $[C_f, C_d, C_\alpha]$ ←compute force error
  $J_k \leftarrow \text{sum}(C_l, C_c, C_\theta, C_{\dot\theta}, C_f, C_d, C_\alpha)$
  $[\mathbf{x}, \mathbf{u}]$ ←minimize(J_k)
return $[\mathbf{x}, \mathbf{u}]$

$\mathbf{x_0}$, **w** ← initialize
while *drawing not finished* **do**
  $\mathbf{p_p}$ ← Measure pen position
  $\mathbf{p}_{\mathbf{p},k}$ ← $KalmanFilter(\mathbf{p_p})$
  $\mathbf{x_0}$ ← update system states, from sensor data
  parameters ← update MPCC parameters
  $[\mathbf{x_{t=1..n}}, \mathbf{u_{t=1...n}}] \leftarrow MPCC(\mathbf{x_0}, \mathbf{w}, \mathbf{p}, \mathbf{params})$
  $\mathbf{x_0} \leftarrow \mathbf{x_1}$
  apply$(\mathbf{u_0})$
end

DIPOLE-DIPOLE MODEL

In this section we describe the derivation of the dipole-dipole model for the in-plane actuation force, as well as the case of considering a pen tilt β of the pen. Please refer to the schematic Figure 6 for vector notations we use in this section.

The coordinate system is given by,

$$\mathbf{e_d} = \frac{\mathbf{p_m} - \mathbf{p_p}}{\|\mathbf{p_m} - \mathbf{p_p}\|} \quad (17)$$

$$\mathbf{e_z} = [0, 0, 1]^T \quad (18)$$

$$\mathbf{e_t} = \mathbf{e_d} \times \mathbf{e_z} \quad (19)$$

with $\mathbf{e_d}$ the in-paper-plane distance from the pen contact point to the electromagnet center projection, $\mathbf{e_z}$ the vertical out-of-plane direction and $\mathbf{e_t}$ the orthogonal vector to the former two.

The dipole-dipole expression for the force acting on $\mathbf{m_p}$ due to $\mathbf{m_m}$ and separated by $\mathbf{r_{mp}}$ is given by Eq. 13), repeated here:

$$\mathbf{F_p} = \frac{3\mu_0}{4\pi r_{mp}^5}\left[\left(\langle \mathbf{m_p}, \mathbf{r_{mp}}\rangle\right)\mathbf{m_m} + \left(\langle \mathbf{m_m}, \mathbf{r_{mp}}\rangle\right)\mathbf{m_p} + \left(\langle \mathbf{m_p}, \mathbf{m_m}\rangle\right)\mathbf{r_{mp}} - \frac{5\left(\langle \mathbf{m_p}, \mathbf{r_{mp}}\rangle\right)\left(\langle \mathbf{m_m}, \mathbf{r_{mp}}\rangle\right)}{r_{mp}^2}\mathbf{r_{mp}}\right], \quad (20)$$

The two dipoles and the vector distance between them can be expressed in the proposed coordinate system as,

$$\mathbf{m_m} = \alpha\, m_m\, \mathbf{e_z} \quad (21)$$

$$\begin{aligned}\mathbf{m_p} &= -(m_p \sin\beta\cos\gamma)\,\mathbf{e_d} \\ &\quad +(m_p \sin\beta\sin\gamma)\,\mathbf{e_t} \\ &\quad +(m_p\cos\beta)\,\mathbf{e_z}\end{aligned} \quad (22)$$

$$\begin{aligned}\mathbf{r_{mp}} &= -(d + h_p \sin\beta\cos\gamma)\,\mathbf{e_d} \\ &\quad +(h_p \sin\beta\sin\gamma)\,\mathbf{e_t} \\ &\quad +(h - (1-\cos\beta)h_p)\,\mathbf{e_z}\end{aligned} \quad (23)$$

and the three scalar products of equation 20,

$$\langle \mathbf{m_m}, \mathbf{r_{mp}}\rangle = \alpha\, m_m[h - (1-\cos\beta)h_p] \quad (24)$$

$$\begin{aligned}\langle \mathbf{m_p}, \mathbf{r_{mp}}\rangle &= mp\,[-\sin\beta\cos\gamma(d + h_p\sin\beta\cos\gamma) \\ &\quad +\sin\beta^2\sin\gamma^2 h_p + \\ &\quad \cos\beta(h - h_p(1-\cos\beta))]\end{aligned} \quad (25)$$

$$\langle \mathbf{m_m}, \mathbf{m_p}\rangle = \alpha m_m m_p \cos\beta \quad (26)$$

Position-aware dipole-dipole model

We first derive the position-aware dipole-dipole model, before continuing to the full position-aware and angle-aware model. We rewrite Eq. 20 with an equivalent pen dipole $\tilde{\mathbf{m}}_\mathbf{p}$, obtained by applying the small tilting angle approximation ($\cos\beta \simeq 1$ and $\sin\beta \simeq 0$) to Eq. 22,

$$\tilde{\mathbf{m}}_\mathbf{p} = m_p\, \mathbf{e_z}\,, \quad (27)$$

where the scalar magnetization is given by $m_p = B_r V/\mu_0$. B_r is the residual magnetization of the permanent magnet and V its volume and $\mathbf{e_z}$ is the z-unit vector. This approximation removes the requirement for tracking the pen tilt. More importantly it drastically simplifies the force equation since both dipoles now only have a z component and thus the actuation only depends on the distance d between pen and magnet (not on β nor γ). This provides a simplified version of the 3D distance vector,

$$\tilde{\mathbf{r}}_\mathbf{mp} = -d\,\mathbf{e_d} + h\,\mathbf{e_z}, \quad (28)$$

where the vertical distance, $h = h_m + h_p$, is constant. Note that the in-plane distance $d = \|\mathbf{p_p} - \mathbf{p_m}\|$ is one of the variables we

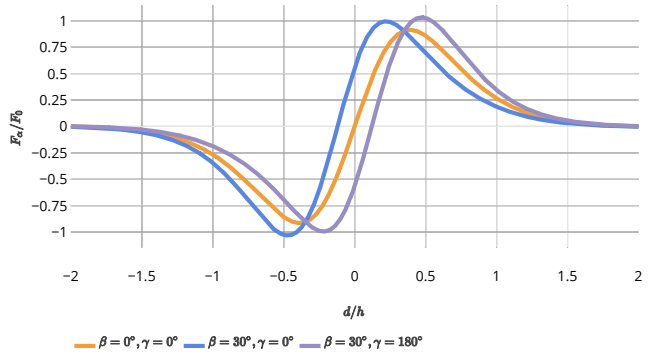

Figure 12. In-plane magnetic force as function of position. The horizontal displacement between curves (each denoting a different pen-tilt) is the approximation error induced by the upright pen (purple) assumption (angles defined in Figure 6).

Table 5. List of electromagnet model and hardware parameters

Name	Value	Description
μ_0	$4\pi\ 10^{-7}$ [H/m]	Vacuum permeability
B_r	1.3 [T]	Pen magnet type (NIB N42)
V	0.66 [cm^3]	Pen magnet volume
m_p	0.683 [A m^2]	pen dipole (= $B_r V/\mu_0$)
m_m	1.286 [A m^2]	electromagnet dipole
h	2.71 [cm]	z-distance $\mathbf{m_m}$ to $\mathbf{m_p}$
h_p	1.40 [cm]	height pen-tip to magnet
h_m	1.31 [cm]	z-distance from plane to $\mathbf{m_m}$.
F_0	0.488 [N]	force factor in Eq. 30

seek to control, given the projections of the pen position ($\mathbf{p_m}$) and the electromagnet position ($\mathbf{p_p}$) onto the sketching plane.

The electromagnet dipole ($\mathbf{m_m}$) is mounted in a fixed upright position. Therefore it can be expressed via Eq. 21, without incurring any approximation error. The magnetization value of the full-strength dipole m_m, which approximates the electromagnet, can be derived experimentally. For this purpose we scan the magnetic field generated by the electromagnet, setting $\alpha = 1$ and using a hall sensor and adjust the parameters of EM field equation to give a good fit, as explained below in section *Electromagnet dipole equivalent*. Table 5 reports the values of m_m, m_p and h that were used in our experiments.

The total force acting on the pen (Eq. 20) can now be decomposed into the in-plane and vertical force components:

$$\mathbf{F_p} = F_a\ \mathbf{e_d} + F_z\ \mathbf{e_z}\ . \tag{29}$$

Here $\mathbf{F_a} = F_a\ \mathbf{e_d}$ represents the quantity we seek to control. By substituting the results form Eq. 21, 27 and 28 into Eq. 20 and maintaining only the in-plane contributions ($\mathbf{e_d}$ direction), we obtain the expression for the actuation force as function of pen-magnet separation:

$$\mathbf{F_a} = \alpha\ F_0 \left(\frac{d\left(4 - \frac{d^2}{h^2}\right)}{h\left(1 + \frac{d^2}{h^2}\right)^{\frac{7}{2}}} \right) \mathbf{e_d}, \tag{30}$$

where F_0 is a constant force parameter given by the expression,

$$F_0 = \frac{3\ \mu_0\ m_p\ m_m}{4\ \pi\ h^4}\ . \tag{31}$$

Fig. 12 illustrates how the dimensionless ratio within parentheses in Eq. 30 governs the force strength as function of distance $d = \|\mathbf{r_d}\|$. The actuation force F_a is zero if the two magnets are aligned with one another ($d = 0$), it has a maximum $F_a^{max} = 0.9F_0$ at $d = 0.39h$, and we can assume there is no more attraction for distances $d > 2h$. In Table 5 we report the value of F_0 we obtained for our prototype.

Note that these simplifications lead only to a small approximation error. Compared to an angle dependent formulation, a tilt of up to $\beta = 30°$ leads to a max error in our model (Eq. 30) equivalent to shifting the distance d by ±3 [mm] (Figure 12).

Angle-aware dipole-dipole model

In this section, we derive the complete EM model, using both, the pen position and its tilting angle as free variables. We continue the deduction of $\mathbf{F_p}$ by substituting Eq. 21—26 into the main expression Eq. 20. However, by following that path we wouldn't necessarily attain information on how strong the actuation force depends on the tilting angles β and γ. Here we take a different path. Based on the geometry of our system, we consider the cases where the pen is tilted by only a small angle. We introduce this small-angle approximation by keeping only the first order terms in β,

$$\sin\beta \approx \beta \quad (\text{with}\ \beta\ \text{in radians}) \tag{32}$$

$$\cos\beta \approx 1 \tag{33}$$

As an indication of what this approximation means, for an angle $\beta = 30°$, the difference between using $\sin\beta$ or $\cos\beta$ or their approximations forms (Eq. 32 and 33) is 5% and 15 %, respectively. Under the small-β approximation, the dipoles' vectors are,

$$\mathbf{m_m} = \alpha\ m_m\ \mathbf{e_z} \tag{34}$$

$$\mathbf{m_p} \simeq -m_p\beta\cos\gamma\mathbf{e_d} + m_p\beta\sin\gamma\mathbf{e_t} + m_p\ \mathbf{e_z} \tag{35}$$

and the distance between dipoles,

$$\mathbf{r_{mp}} \simeq -(d + h_p\beta\cos\gamma)\ \mathbf{e_d} + h_p\beta\sin\gamma\ \mathbf{e_t} + h\ \mathbf{e_z} \tag{36}$$

with the length of that distance, at first order on β,

$$r_{mp} \simeq d^2 + h^2 + 2dh_p\beta\cos\gamma \tag{37}$$

In turn, the scalar products (Eq. 24—26) can be written as,

$$\langle \mathbf{m_m}, \mathbf{r_{mp}} \rangle \simeq \alpha\ m_m h \tag{38}$$

$$\langle \mathbf{m_p}, \mathbf{r_{mp}} \rangle \simeq mp\ [-\beta\cos\gamma d + h] \tag{39}$$

$$\langle \mathbf{m_m}, \mathbf{m_p} \rangle \simeq \alpha\ m_m m_p \tag{40}$$

We can now substitute these expressions into the main force equation 20. As we do in previous section, we consider only the terms that contribute to the component $\mathbf{e_d}$ of the force.

Keeping only these terms that contain β up to the first order,

$$\mathbf{F_p^{(d)}} = \frac{3\mu_0\alpha m_m m_p}{4\pi r_{mp}^5}\left[-d + \frac{5dh^2}{r_{mp}^2} - h\beta\cos\gamma - h_p\beta\cos\gamma + \right. \\ \left. + \frac{5h^2 h_p\beta\cos\gamma}{r_{mp}^2} - \frac{5hd^2\beta\cos\gamma}{r_{mp}^2}\right]\mathbf{e_d} \quad (41)$$

$$= \frac{3\mu_0\alpha m_m m_p}{4\pi(h^2+d^2)^{5/2}}\left[\frac{-d(d^2+h^2)+5dh^2}{(h^2+d^2)} + \right. \\ \left. \beta\cos\gamma\left(-h - h_p + \frac{5(h^2h_p - hd^2)}{(h^2+d^2)} - \frac{5d^2h^2h_p}{(h^2+d^2)^2}\right)\right]\mathbf{e_d} \quad (42)$$

$$\mathbf{F_p^{(d)}} = \alpha\, F_0\, [\, f_0(d) \,+\, \beta\cos\gamma\, f_1(d)\,]\, \mathbf{e_d} \quad (43)$$

where we define,

$$F_0 = \frac{3\,\mu_0\, m_p\, m_e m}{4\,\pi\, h^4}\,. \quad (44)$$

$$f_0(d) = \frac{d\left(4 - \frac{d^2}{h^2}\right)}{h\left(1+\frac{d^2}{h^2}\right)^{\frac{7}{2}}} \quad (45)$$

$$f_1(d) = \frac{1+\frac{h_p}{h}}{\left(1+\frac{d^2}{h^2}\right)^{\frac{5}{2}}} + \frac{5\left(\frac{h_p}{h}+\frac{d^2}{h^2}\right)}{\left(1+\frac{d^2}{h^2}\right)^{\frac{7}{2}}} - \frac{5\left(\frac{h_p}{h}\right)\left(\frac{d^2}{h^2}\right)}{\left(1+\frac{d^2}{h^2}\right)^{\frac{9}{2}}} \quad (46)$$

Note that by considering the case $\beta = 0$ in Eq. 43, we recover what we obtain for $\mathbf{F_a}$ as calculated in Eq. 30. That means that the equation for $\mathbf{F_p^{(d)}}$ subsumes the cases of the pen being tilted by a small angles, and it can be used in future EM actuated systems which may be able to track β and γ.

ELECTROMAGNET DIPOLE EQUIVALENT

Here we describe the experimental validation of the dipole model for our electromagnet, that allows us to compute the force that the electromagnet exerts onto the permanent magnet on the pen. . The magnetic field generated by a dipole $\mathbf{m_m}$ (electromagnet) at the position of dipole $\mathbf{m_p}$ (pen) can be written as,

$$\mathbf{B_m}(\mathbf{r_{mp}}, \mathbf{m_m}) = \frac{\mu_0}{4\pi}\left(\frac{3\mathbf{r_{mp}}\left(\mathbf{m_m}\cdot\mathbf{r_{mp}}\right)}{r_{mp}^5} - \frac{\mathbf{m_m}}{r_{mp}^3}\right) \quad (47)$$

where the vector $\mathbf{r_{mp}}$ is the vector that goes from $\mathbf{m_m}$ to $\mathbf{m_p}$ (see Figure 6). The magnetic field $\mathbf{B_m}$ is well described in a cylindrical system centered on the dipole and with the z-axis aligned on the direction of $\mathbf{m_m}$. Taking only the z component on Eq. 47 and using the definitions of $\mathbf{r_{mp}}$ (Eq. 28) and $\mathbf{m_m}$ (Eq. 21) we arrive at,

$$B_{m,z}(d) = \frac{\mu_0\alpha m_m}{4\pi}\left(\frac{2h^2 - d^2}{(d^2+h^2)^{\frac{5}{2}}}\right) \quad (48)$$

We measure the z-component of the magnetic field generated by the electromagnet to compare it with the dipole prediction of Eq. 48. We use a hall sensor (Allegro A1324, sensitivity is 5 mV/G) to measure the z-magnetic flux at a fix height h_m, where the magnet of the pen would be. Setting the electromagnet to $\alpha = 1$ and moving it in a grid we attain multiple readings of the hall sensor for different electromagnet positions $\mathbf{p_m}$. We present the obtained magnetic field plotted in Figure 13, top.

Due to symmetry over the z-axis we expect for $B_{m,z}$, we re-plot all points as a function of distance $d_s = \|\mathbf{p_s} - \mathbf{p_m}\|$, with $\mathbf{p_s} = (0,0)$ the in-plane position of the hall sensor. In turn, Eq. 48 can be expressed in the form,

$$B_{m,z}(d_s) = C_1\frac{2C_2^2 - d_s^2}{\left(d_s^2 + C_2^2\right)^{5/2}} \quad (49)$$

where we have defined two parameters used for the fitting,

$$C_1 = \frac{\mu_0\alpha m_m}{4\pi} \quad (50)$$

$$C_2 = h \quad (51)$$

The bottom plot of Figure 13 shows the measured data for magnetic flux $B_{m,z}(d_s)$ and the fitting to Eq. 49, from which we obtained $C_1 = -1.276\ 10^{-07}$ and $C_2 = 2.713\ 10^{-02}$. By replacing these values in equations 50 and 51, we observe that our system can be described by the values $m_m = 1.286$ [A m^2] and $h = 2.71$ [cm]. We want to emphasize the excellent agreement in Figure 13 between the experimental values and the proposed dipole model for the electromagnet. However, we should note that the experimental points show a flattening of $B_{m,z}(x)$ for values of $x < 3$ [mm], that translates into smaller values of forces in that region, as $\mathbf{F_a} \propto \nabla B_{m,z}$.

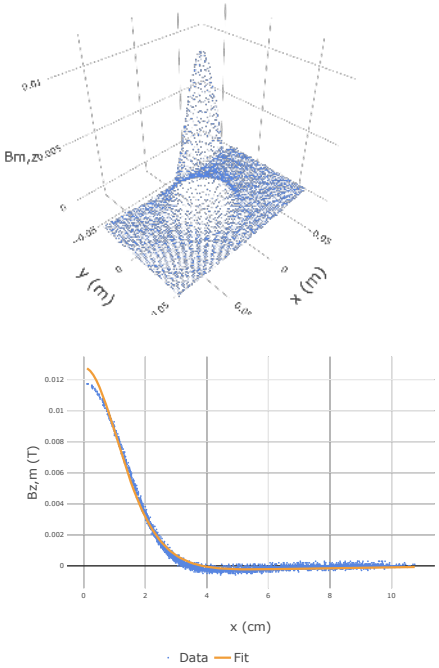

Figure 13. 3D overview of all data points. The x,y axis are position and the z-axis is $B_2^{(z)}$